Where Quantum and Fluids entangle

Quantum Computational Fluid Dynamics
Core Benchmark CFD Set
Project number 101080085

Call:	HORIZON-CL4-2021-DIGITAL-EMERGING-02
Topic:	HORIZON-CL4-2021-DIGITAL-EMERGING-02-10
Type of action:	HORIZON Research and Innovation Actions
Granting authority:	European Commission-EU
Project starting date: fixed date:	1 November 2022
Project end date:	31 October 2026
EU-Project duration:	48 months
Project Coordinator:	University of Hamburg (UHH)
Work Package Leader	Technical University of Hamburg (TUHH)
Cooperations	University of Hamburg (UHH), ENGYS (ENG)
Deliverable number:	D1.1
WP contributing to the deliverable:	WP#1 Core CFD Examples and Algorithms
Deliverable Type:	Data
Revision:	2
Dissemination level:	Public
Due Submission date:	30.04.2024
Prepared By:	TUHH, UHH, ENG
Internal Reviewers:	DJ, TR, PO, SB, EdV
Final Approval:	

This project receives funding from the European Union's Horizon 2020 HORIZON Research and Innovation Actions Program under Grant Agreement #101080085

Revision History

Version	Date	Who	Changes
V1.0	30.04.24	DJ, TR, PO, SB	Creation and publication of the document.
V2.0	11.01.25	DJ, TR, PO, SB, EdV	Revision

Executive Summary

The Quantum Computational Fluid Dynamics (QCFD) project is dedicated to advance quantum computing for Computational Fluid Dynamics (CFD) simulations and their use in industry.
The deliverable D1.1 provides input to other work packages as part of Work Package 1 (WP1) ("Core examples and algorithms for CFD"). This includes a collection of elementary CFD benchmarks as well as first application-oriented examples and their solutions based on conventional CFD methods, which are partly flanked by additional quantum-based solutions.

In accordance with the data management plan (DMP), D1.1 follows the FAIR data principles – findability, accessibility, interoperability and reusability – the associated datasets are provided with a detailed metadata structure, unique identifiers and the corresponding documentation. This ensures that the data is easily accessible and usable by third parties. Public access is granted via a dedicated research data repository (FDR) hosted at the University of Hamburg (UHH), www.fdr.uni-hamburg.de/communities/qcfd/. To make it easier for users to keep track, all datasets belonging to the project are collected in a QCFD community group on the mentioned data server.

This project receives funding from the European Union's Horizon 2020 HORIZON Research and Innovation Actions Program under Grant Agreement #101080085

Content

This project receives funding from the European Union's Horizon 2020 HORIZON Research and Innovation Actions Program under Grant Agreement #101080085

List of abbreviations

Acronym / Short Name	Meaning
BEV	Battery Electric Vehicle
CA	Consortium Agreement
CFD	Computational Fluid Dynamics
CFL	Courant-Friedrichs-Levy criteria
D	Deliverable
DMP	Data Management Plan
DOI	Digital Object Identifier
EC	European Commission
ENG	ENGYS SRL
EU	European Union
FD	Finite Difference
FDR	Research Data Repository
FV	Finite Volume
FZL	Jülich Research Centre
KPI	Key Performance Indicator
LES	Large-Eddy Simulation
MPS	Matrix Product States
NS	Navier Stokes
PlanQC	PlanQc GMBH
PO	Project Officer
QCFD	Quantum Computational Fluid Dynamics
RANS	Reynolds Averaged Navier Stokes
VQA	Variational Quantum Algorithm
TR	Technical Readiness
TUHH	Technical University of Hamburg
TUC	Technical University of Crete
TUM	Technical University of Munich
UHH	University of Hamburg
WP	Work Package
WPL	Work Package Leader

This project receives funding from the European Union's Horizon 2020 HORIZON Research and Innovation Actions Program under Grant Agreement #101080085

1 Introduction

The rise of digital computers has made CFD an indispensable tool in today's engineering fluid mechanics. As a first step, the D1.1 result provides CFD data obtained from classical grid-based CFD methods as a benchmark for quantum CFD algorithms.

It is important to understand the TR-level of quantum CFD and the nature of the algorithms. When creating test cases, we considered the limitations of quantum algorithms and hardware, which represents the state of the art at the time of compiling the deliverable. Quantum hardware-based strategies [1, 2, 3, 4] are currently still very expensive for hardware reasons, which is why a coarse resolution was preferred for the development of the corresponding algorithms and their benchmarking. It is for this reason that none of the applications proposed here are complex relative to the current state of classical CFD (although it is planned that they will become so in future). Hence, when we speak of ”advanced” or ”complex”, this is often relative to coarse grid scalar transport equation and elementary examples provided in D1.1 are designed to match what is achievable in QCFD on a one-to-one basis in terms of integration points and physics. On the contrary higher resolutions are possible in conjunction with quantum-inspired approaches [5, 6], e.g., Matrix-Product-State (MPS) methods, and quantum computers do not necessarily have to be used. The cases documented in D1.1 aim to serve both strategies which underpins the multi-directional research of the project. Within a best-case scenario QCFD could be capable of solving complex multi-physical problems as they, e.g., occur in the battery design of battery electric vehicles (BEV), where a generic case has been added to D1.1.

Due to the strong links of quantum algorithms with established CFD approaches, which are inherent components of quantum-based algorithms, the consortium considers comparison with classical methods and (if possible) analytical solutions to be essential, especially for lower resolutions. This is because the details of the convergence process are as important to the development of the quantum algorithms as the absolute accuracy of the results and might provide insight into the more nuanced facets and sub-components of the algorithms.

Mind that there are no standard practices in quantum computing for solving CFD problems. We would like to point out, that issues surrounding the definition of scalable quantum algorithms and quantum computing hardware/ emulation limit the resolution as well as the complexity achievable by quantum algorithms at this stage. We believe that there is no point in comparing quantum performance to classical performance at this stage since the quantum algorithms are incomplete, un-optimized and generally at a low maturity level. Quantum advantage is additionally only expected to become pronounced at scale. The objective of D1.1 is thus not to compare performance, but to assist the development of the quantum CFD algorithms. Effort comparisons with CFD results are not to be expected at the time of compiling the deliverable, since QCFD and its hardware are not ready for comparability. Hence, the data provides a basis for evaluating methodological differences but does not give information on the quantum hardware performance.

Dataset-specific documentation to support the interpretation and outline the usability of the data is given. Furthermore, the datasets are accompanied by metadata, including parameters, software versions, library dependencies, and simulation time frames. Lastly, the data sets are enhanced by a keyword-based search system incorporating Digital Object Identifiers (DOIs). With this documentation process, we intend to guarantee the replication of our (and other) methods and promote accessibility to the scientific and industrial sectors. The complete data is made available, according to the submitted Data Management strategy, in a dedicated research data repository (FDR) hosted at the university of Hamburg (UHH), www.fdr.uni-hamburg.de/communities/qcfd/, and associate within the project community QCFD.

This project receives funding from the European Union's Horizon 2020 HORIZON Research and Innovation Actions Program under Grant Agreement #101080085

2 Data Description

Deliverable 1.1 aims to support the analysis of newly developed QCFD methods and to provide a comparison with CFD datasets obtained from classical, established mesh-based Finite Difference (FD) or Finite Volume (FV) simulation methods. Where available, the quantum results obtained in the project and their publications are listed as an additional dataset. The data source (FD, FV or QCFD) is clearly indicated in the report and the dataset.

To reduce the level of complexity, only structured grid examples are considered. Moreover, the document distinguishes between the (a) the spatial dimension of the problem, (b) the time-dependency of the problem, (c) the amount of (coupled) equations – i.e., single/multi-physics approach, (d) the non-/linearity of the underlying equation, (e) the influence of turbulence, (f) the available number of different resolutions/grids, (g) the scientific and the industrial relevance, (h) the availability of QCFD results and (i) the specific focus of the case.

This reminder of this Section defines the data processing pipeline, the quality/accuracy requirements as well as the suggested performance indicators, e.g., fail/pass criteria, cf. Sec. 2.2.

2.1 Accuracy

Data accuracy is fundamental to meaningful benchmarking and is therefore a key consideration. In this context, the following guidelines are used:

- List of file formats with the corresponding accuracy, accessible without compression
    - Fortran std file format
    - openfoam std file format
    - ...
- Double-precision floating-point number format
- For complex numbers, the 53-bit significant precision of 16 decimal digits is divided between real and imaginary parts.

2.2 Assessment Criteria

For benchmarking purposes, all cases are designed to evaluate the comparison results based on the following criteria:

- Absolute Error: Measure of the deviation between two paired variables.
- l_2- (or Euclidean) norm: In general, a norm consists of a function mapping from a vector space to a non-negative real number. In particular, the l_2-norm is defined as the square root of the scalar product of a vector with itself.
- Fidelity: Often understood as a similarity measure and formed by the scalar product of two normalized vectors.
- Trace Distance: Measure of how distinguishable two (quantum) states are. For pure quantum states, the trace distance is defined as the square root of one minus fidelity.

3 Cases

This Section discusses the currently available benchmark cases of the D1.1. These have been chosen to be representative of different (Q)CFD research branches.

The cases are divided into three main categories according to their spatial dimension, i.e., indicative 1D textbook cases, 2D and 3D applications. Each category is divided into subsections containing different benchmarks that are uniquely identified by an individual DOI.

Note that compressibility of the fluid is neglected in all cases due to the small Mach numbers of $Ma < 0.1$, where the Mach number $Ma = u/a$ indicates the relation between flow speed u and the speed of sound a.
The individual numerical experiments are characterized by non-dimensional parameters, in particular the

- Reynolds number $Re = uL/\nu = \frac{\text{inertial force}}{\text{viscous force}}$ (u: characteristic velocity, L: characteristic length, ν: kinematic viscosity)
- Nusselt number $Nu = hL/k = \frac{\text{convective heat transfer}}{\text{conductive heat transfer}}$ (h: heat transfer coefficient, L: characteristic length, k: thermal conductivity)
- Peclet number $Pe = uL/\Gamma = \frac{\text{advection transport}}{\text{diffusive transport}}$ (u: characteristic velocity, L: characteristic length, Γ: kinematic diffusivity).

For time-dependent or pseudo time-dependent problems, the numerical procedures are additionally characterized by Courant-numbers, also known as CFL numbers, i.e., $C_c = u\Delta t/\Delta x$ for convection and $C_d = \nu\Delta t/\Delta x^2$ for diffusion. Here Δt refers to the employed time step that is used to advance the simulation and Δx represents a typical (local) grid spacing.

3.1 1D Textbook Cases

This first category covers simple steady and unsteady heat conduction problems, fully developed (laminar) shear flows and other well-known 1D examples for single governing differential equations using Finite Volume (FV) and Finite Difference (FD) methods. These cases focus on the development of the QC (not quantum-inspired) algorithms. Discretizations are relatively coarse in order to limit hardware requirement and ensure the applicability of the benchmark data to current quantum hardware.

A detailed description for the corresponding numerical experiments is given below. Note that, in general, the density ρ $[kg/m^3]$ and the viscosity ν $[m^2/s]$ were both set to 1 to obtain the data provided. Moreover, all but one case employ an equidistant spacing and the presented cases do not cover a grid sensitivity analysis.
Table 1 summarizes the features of the 1D test cases including a brief outline of the respective focus and the engineering relevance. The focal points refer to (1) boundary condition, (2) non-homogeneous advection, (3) unsteady effects, (4) advection-diffusion interplay and (5) nonlinear effects. The governing equation refers to diffusion (D) diffusion reaction (DR), unsteady diffusion (uD), unsteady advection diffusion (uAD), steady advection diffusion (AD), and unsteady convection diffusion (uCD) problems. In addition to the classical methods (FD/FV), the Table also contains possibly additional results obtained from QC methods (Q).

Textbook Cases	Eqn.	Spatial	Temporal	# Eqn.	non/linear	Flow	# Grids	Num.	Focus	Ind. Relev.
Shear Flows	D/DR	1D	steady	1		laminar	-	FD	-	10%
Heat Conduction	uD	1D	un/steady	1		laminar	-	FD+Q	(1,3)	25%
Nozzle Flow	uAD	1D	steady	1	linear	laminar	-	FV	(2,3)	15%
Wave Equation	uD	1D	unsteady	1	linear	laminar	-	FD+Q	(3)	10%
Adv.-Diff. Problem	AD	1D	steady	1	linear	laminar	-	FD+Q	(4)	25%
Burgers Equation	uCD	1D	unsteady	1	nonlinear	laminar	-	FD+Q	(5)	30%

TABLE 1: SUMMARY OF SELECTED 1D CASES (3.1).

This project receives funding from the European Union's Horizon 2020 HORIZON Research and Innovation Actions Program under Grant Agreement #101080085

3.1.1 Unidirectional Shear Flows (FV)

Fully developed unidirectional shear flows are classical one-dimensional benchmark flows. The response of a simulation procedure to shear is crucial, since it relates to the wall shear stress and the fluid dynamic drag of obstacles.

The first case is concerned with a plane Couette flow, describable by

$$\nu \frac{\partial^2 u}{\partial y^2} = 0.$$

It refers to an infinitely long resting horizontal bottom wall and a corresponding moving horizontal top wall in a horizontal periodic arrangement (cf. Figure 1). The top wall moves with a unit velocity $\overline{u_p} = 1\ [m/s]$ in horizontal direction. The flow is considered fully developed, and the velocity does not change along the horizontal direction. Due to the fully developed state, the influence of convective terms vanishes $(Pe, Re \to 0)$. Emphasis is thus restricted to a velocity profile along the 1D vertical axis, i.e., along the gap of size $2\delta = 0.2\ [m]$ between the two walls. The considered Reynolds number reads $Re = 2\,\overline{u_p}\delta/\nu = 0.2$, using a unit kinematic viscosity $\nu = 1\ [m^2/s]$.

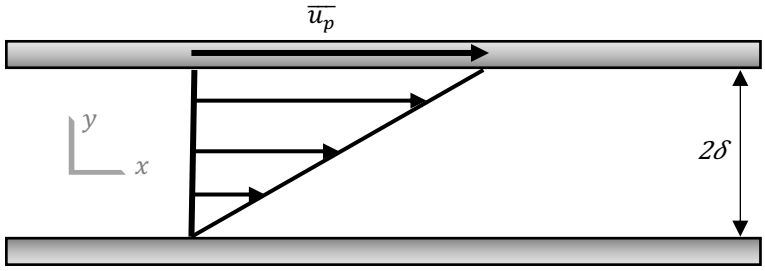

FIGURE 1: SCHEMATIC OF THE PLANE COUETTE FLOW (3.1.1).

The 1D domain is discretized using 10 homogeneous interior cells along the vertical of equidistant height $\Delta y = 0.02\ [m]$. Dirichlet conditions for velocity are assigned to zero (bottom wall) and $\overline{u_p}$ (top wall). Spatial derivatives of the diffusive terms employ central differencing. Results are available via DOI 10.25592/uhhfdm.14201.

Discretization: equidistant in space
Features: 1D, steady, diffusive scalar transport with Dirichlet conditions
Output: $u(y_i, t_k)$

A second case refers to a plane channel flow, viz.

$$\frac{1}{\rho}\frac{\partial p}{\partial x} - \nu \frac{\partial^2 u}{\partial y^2} = 0,$$

where u is a velocity, ν is a (unit) kinematic viscosity, ρ is a (unit) density and $\partial p/\partial x$ is a given pressure gradient. It distinguishes from the previously covered Couette flow, as the flow is not driven by a moving wall, but a (given) constant horizontal pressure gradient. The unidirectional velocity profile is again considered to be fully developed, and convective fluxes are without influence $(Pe, Re \to 0)$. The setup is depicted in Figure 2 and again only involves a 1D domain in the direction of the vertical axis between the two walls.

This project receives funding from the European Union's Horizon 2020 HORIZON Research and Innovation Actions Program under Grant Agreement #101080085

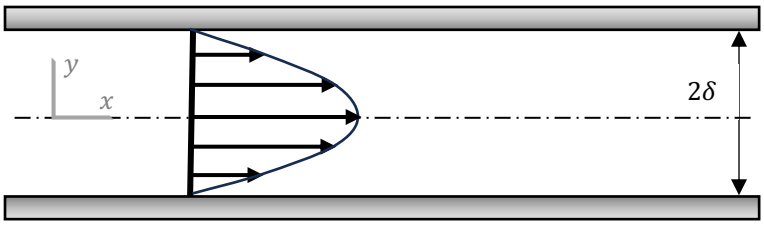

FIGURE 2: SCHEMATIC OF A PLANE CHANNEL FLOW (3.1.1).

The (laminar) flow is symmetric to the horizontal center axis and the numerical model covers only half the domain. The cross-section is parameterized by $\delta = 2/3\ [m]$. The bulk velocity $\overline{u_p}$, i.e., the average horizontal velocity is set to $1\ [m/s]$. The smallest near wall cell is of height $\Delta y_1 = 0.02\ [m]$ and 12 cells are used to mesh the half-height δ. Towards the centerline the discretization is recursively coarsened by $3\Delta y_{i+1} = 4\Delta y_i$. Spatial derivatives of the diffusive terms employ central differencing. Results obtained for a Reynolds number of $Re = 2\,\overline{u_p}\delta/\nu = 4/3$ are available via DOI 10.25592/uhhfdm.14201.

Discretization: equidistant in space
Numerics: FD (2nd-order central in space)
Features: 1D, steady, diffusion-reaction scalar transport with Dirichlet and symmetry conditions
Output: $u(y_i, t_k)$

3.1.2 Steady and Unsteady Heat Conduction (FD/QCFD)

The heat conduction represents an initial step towards the analysis of scalar transport problems. The governing Poisson type partial differential equation describes the (unsteady) processes at $Pe, Re = 0$, i.e., advancing a balance between reaction and diffusion influences. Modeling these physical phenomena is a first milestone that needs to be reached during the development of novel algorithms.
The test case serves as an ideal candidate to verify the quality of the implementation for a wide range of technical boundary conditions, and the deliverable covers both steady and unsteady problems with various boundary conditions. Simulations solve the differential equation

$$\frac{\partial y}{\partial t} - \alpha \frac{\partial^2 y}{\partial x^2} = 0$$

for a unit thermal diffusivity $\alpha = 1\ [m^2/s]$. All results refer to a 1D spatial domain given by the unit interval $x \in [0, 1]\ [m]$ and an equidistant spatial step size Δx. Different interior domain points N_p are employed that correspond to the different numbers of qubits n, i.e., $N_p = 4\ (n = 2)$ to $N_p = 16\ (n = 4)$ with $\Delta x = 1[m]/(N_p + 1)$. Spatial derivatives employ central differencing. For unsteady cases, time is also discretized equidistantly using a 1st-order backward scheme and a constant time step that ensures of C_d=0.5 for all spatial employed discretizations featuring different time instant numbers to cover the simulation period.

The boundary settings include the combinations of (left-right) Dirichlet-Dirichlet, Neumann-Neumann, Dirichlet-Neumann, Robin-Robin, and periodic boundary conditions. For the sake of completeness, Table 2 gives an overview and defines the boundary conditions for the dependent variable y (where different values for a, b, c were used).

Boundary Setting	**Condition**
Dirichlet - Dirichlet	$y(x=0) = a, \quad y(x=1) = b$
Neumann - Neumann	$\partial y/\partial x\,|_{x=0} = a, \quad \partial y/\partial x\,|_{x=1} = b$
Dirichlet - Neumann	$y(0) = a, \quad \partial y/\partial x\,|_{x=1} = b$

This project receives funding from the European Union's Horizon 2020 HORIZON Research and Innovation Actions Program under Grant Agreement #101080085

Robin - Robin	$ay(x=0) + {\partial y}/{\partial x}\,|_{x=0} = c,$ $by(x=1) + {\partial y}/{\partial x}\,|_{x=1} = c$
Periodic	$y(x=0) = y(x=1)$

TABLE 2: BOUNDARY SETTINGS USED FOR CASE (3.1.1).

Available data involves classical FD results for steady and unsteady heat conduction and companion VQA results which were published in the Computers and Fluids engineering CFD journal [2]. The data can be found under DOI 10.25592/uhhfdm.14123.

Discretization: equidistant in space and time
Numerics: FD (1st-order backward in time, 2nd-order central in space)
Features: 1D, unsteady, diffusive scalar transport featuring a variety of engineering boundary conditions
Output: $y(x_i, t_k)$

3.1.3 Nozzle Flows (FV)

The nozzle flow simulates the geometry depicted in Figure 3 to compute the passive scalar transport equation

$$\frac{\partial \phi}{\partial t} + u\frac{\partial \phi}{\partial x} - \nu\frac{\partial^2 \phi}{\partial x^2} = 0.$$

Convection is taken into account, i.e., $Pe \neq 0$, however the case is linear and the velocity u is prescribed throughout the domain using mass conservation arguments. A Dirichlet value $\phi = 1$ is set at the left inlet boundary where the (prescribed) velocity reads $u_{\text{inlet}} = 2\ [m/s]$. The right outlet boundary is described by a zero-gradient Neumann condition for ϕ, i.e., a vanishing derivative normal to the exit (outlet) plane. The remaining two horizontal boundaries are also assigned to zero gradient conditions.

The Reynolds number, based on the inlet velocity and the nozzle length, reads $\mathrm{Re} = u_{\text{inlet}}\, L/\,\nu = 2$. The horizontal extension of the domain reads $x \in [-1, +1\,][m]$. The symmetric geometry depicts a linear variation of the cross-section, cf. Figure 3. The top wall is specified by the two points $(x = -1, y = 1\,)$ to $(x = 1, y = 0.5\,)$, similarly, the bottom wall can be defined by $(x = -1, y = -1\,)$ to $(x = 1, y = -0.5\,)$. The prescribed velocities in each cross section u_i follow from the continuity relation $u_i \cdot Area_i = u_{\text{inlet}} \cdot Area_{\text{inlet}}$. The cell-centered FV scheme employs 10 control volumes with an equidistant horizontal extension of $\Delta x = 0.2\ [m]$.
Integrals are approximated using a second-order accurate mid-point rule. Spatial derivatives of the diffusive terms employ central differencing. Convective derivatives employ a 2nd-order linear upwind differencing scheme and time is approximated with 1st-order backward differences. Simulations employ a constant timestep of $\Delta t = 0.0001\ [s]$ over $3\ [s]$, recording every 100th time instant. The data is available under DOI 10.25592/uhhfdm.14203.

Features: Unsteady, linear 1D scalar convection-diffusion with engineering boundary conditions
Numerics: FV (1st-order backward in time, 2nd-order central for diffusion, 2nd-order upwind for advection)
Grid: The grid employs equidistantly spaced control volumes. Time steps are also equidistant.
Output: Recordings of the scalar field $\phi(x_i, t_k)$ for every 100th time step starting from $t = 0\ [s]$.

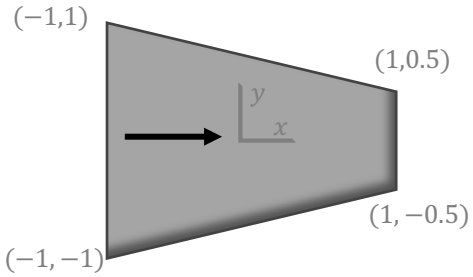

FIGURE 3: SCHEMATIC EXAMPLES OF NOZZLE FLOWS (3.1.3).

3.1.4 Wave Equation (FD/QCFD)

This application addresses a linear transport phenomenon governed by the wave equation

$$\frac{\partial^2 y}{\partial t^2} - c^2 \frac{\partial^2 y}{\partial x^2} = 0,$$

for the displacement $y\ [m]$ under the influence of a constant propagation speed is $c = 1\ [m/s]$. The left and right boundary of the 1D unit domain $x \in [0, 1\,]\ [m]$ are assigned to homogenous Dirichlet boundary conditions $y(x = 0) = y(x = 1) = 0$. The time implicit simulation describes the evolution of an initial Gaussian distribution $y_0 = \exp\,(-(10x - 3.5)^4)$ over $N_T = 30$ time steps, cf. Figure 4.
Time is discretized with a fixed time step of $\Delta t = 0.05\ [s]$. Similarly, spatial discretization employs a constant spacing $\Delta x = 1\ [m]/(N_p + 1)$ for $N_p = 64$ interior points, i.e., $n = 6$ qubits, using a FD approach. The temporal derivative is approximated with first-order backward differences and the spatial derivative is discretized using a second-order central differences.
Available data involves classical FD and companion VQA results. The data is available under DOI 10.25592/uhhfdm.16634.

Features:	Unsteady, linear 1D scalar wave eqn. with Dirichlet boundary conditions
Numerics:	FD (1st-order backward in time, 2nd-order central in space)
Grid:	The grid employs equidistant spatial and temporal step sizes
Output:	Recordings of the scalar field $y(x_i, t_k)$ for the initial 30 time steps

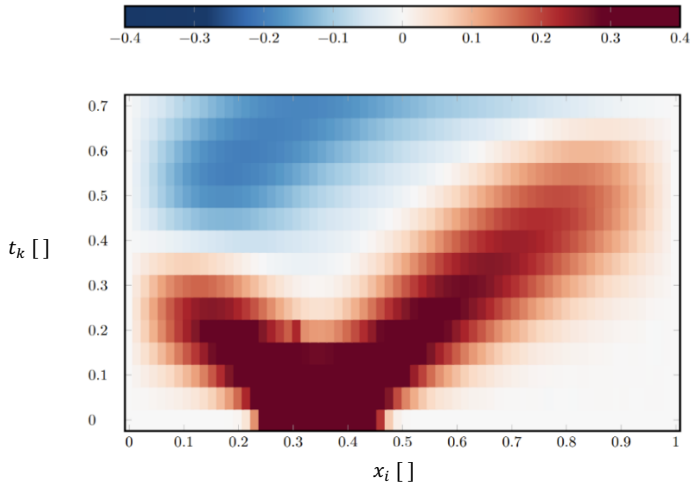

FIGURE 4: EXEMPLARY RESULTS FOR THE WAVE EQUATION (3.1.4).

This project receives funding from the European Union's Horizon 2020 HORIZON Research and Innovation Actions Program under Grant Agreement #101080085

3.1.5 Steady Advection-Diffusion Problem (FD/QCFD)

As the approximation of the convective kinematics and the interplay between convection and diffusion is crucial for engineering applications, the steady advection-diffusion equation for the transport of a scalar property ϕ is

$$u\frac{\partial \phi}{\partial x} - \Gamma\frac{\partial^2 \phi}{\partial x^2} = 0,$$

which is a relevant benchmark. To this end, investigations assume a constant velocity $u = 1\ [m/s]$ as well a different constant diffusivity values $\Gamma\ [m^2/s]$, and a unit interval $x \in [0,1][m]$. The generic scalar ϕ is subject to Dirichlet boundary conditions $\phi(x = 0) = 0$ and $\phi(x = 1) = 1$.
The ratio of the convective and diffusive transport indicates the nature of the problem and is quantified by the local Peclet number $Pe_{\Delta x} = u\Delta x/\Gamma$, where Δx is the local grid size. For the domain and boundary conditions considered, the analytical solution to the problem reads $\phi(x) = [\exp(Pe_{\Delta x}\, x/\Delta x) - 1]/\,[\exp\,(Pe_{\Delta x} L/\Delta x) - 1]$, cf. [7]. Exemplary results are illustrated in Figure 5.

Two FD results are added to D1.1. The first result covers a diffusion dominant case, cf. $Pe_{\Delta x} = 0.3$. The second an advection dominant case, i.e., $Pe_{\Delta x} = 30$. The approximation of diffusive derivatives employs 2nd-order central differences. The convective derivative employs either 2nd-order central schemes, a 1st-order upwind differencing scheme (UDS), a 2nd-order linear-upwind differencing scheme (LUDS) or a 3rd order QUICK scheme. The domain is discretized with $N_p = 16$ interior points, i.e., $n = 4$ qubits, with $\Delta x = 1\ [m]/(N_p + 1)$.
The FD results and results from a VQA simulation are accessible for validation via DOI 10.25592/uhhfdm.16634.

Features: linear 1D advection-diffusion equation with Dirichlet boundary conditions
Numerics: FD (different central & upwind-biased convective approximation & central diffusive approximation)
Grid: The grid employs equidistant spatial sizes
Output: Recordings of the scalar field $\phi(x_i)$

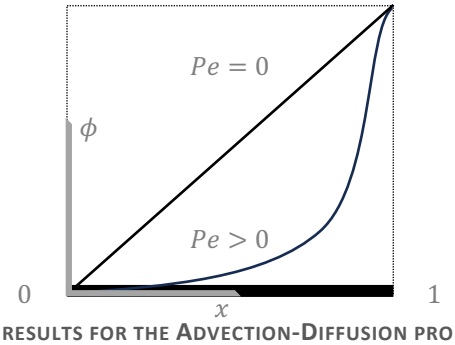

FIGURE 5: EXEMPLARY RESULTS FOR THE ADVECTION-DIFFUSION PROBLEM, CF. [7], (3.1.5).

3.1.6 Burgers' Equation (FD/QCFD)

The 1D Burger's equation is a nonlinear differential equation that considers convective influences, i.e., $Pe, Re \neq 0$,

$$\frac{\partial u}{\partial t} + u\frac{\partial u}{\partial x} - \nu\frac{\partial^2 u}{\partial x^2} = 0,$$

where u is a velocity and ν is a viscosity. The equation is often used as a simplified Navier-Stokes model and has applications in areas such as shock waves, turbulence, and traffic flow. Studies employ a one-dimensional unit domain $x \in [0, 1]\ [m]$, with an equidistant spatial step size $\Delta x = 1[m]/(N_p + 1)$. The domain is discretized using

This project receives funding from the European Union's Horizon 2020 HORIZON Research and Innovation Actions Program under Grant Agreement #101080085

$N_p = 64$ interior points, which corresponds to $n = 6$ qubits. The temporal space is also equidistantly discretized using a 1st-order backward scheme.

Two different Reynolds numbers are considered, cf. Figure 6. The first case is concerned with an inviscid case with a Dirichlet (inflow) condition with velocity of 2 $[m/s]$ at the left end and zero gradient (Neumann) conditions at the right end. Time discretization follows from C_c=0.6 based on a reference velocity of 2 $[m/s]$. The second case computes a viscous case at $Re = 100$ featuring periodic boundary conditions. The case observes a non-centered initial velocity distribution of a Gaussian pulse with a unit peak velocity. Time discretization follows from C_c=1.0 based on the unit velocity.

Access to the data is provided under DOI 10.25592/uhhfdm.16634.

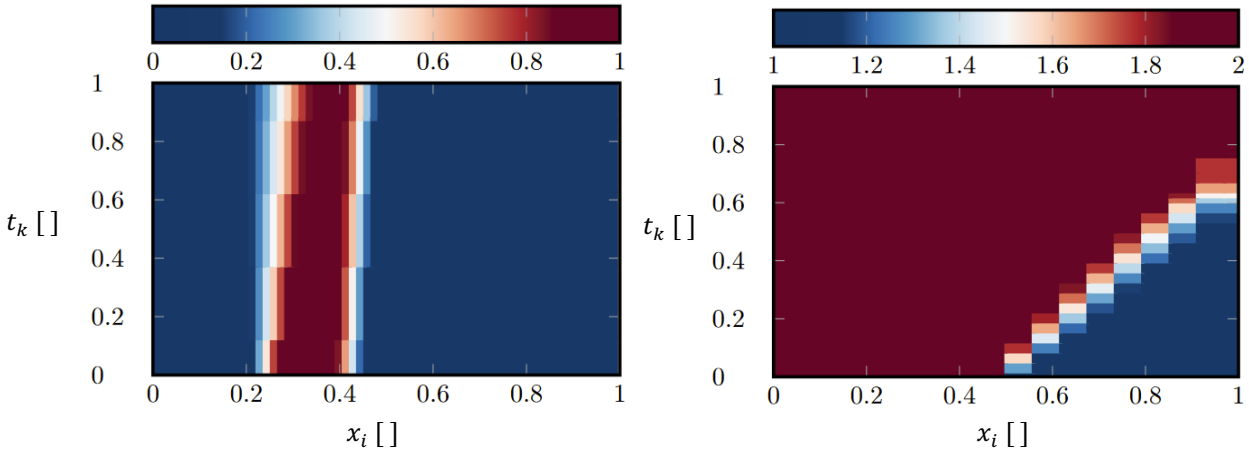

FIGURE 6: RESULTS FOR THE CONSIDERED TWO 1D BURGERS EQUATION CASES (LEFT: VISCOUS CASE; RIGHT: INVISCID CASE) (3.1.6).

Spatial derivatives of the diffusive terms employ central differencing whereas first-order upwind differences are used to approximate the convective derivative. Time derivatives follow from a first-order backward scheme.

Discretization: equidistant in space and time
Numerics: FD (2nd-order central differences for diffusion; 1st-order upwind differences for convection, 1st-order backward in time)
Features: 1D, unsteady, nonlinear convection-diffusion scalar transport with different boundary conditions
Output: $u(x_i, t_k)$

This project receives funding from the European Union's Horizon 2020 HORIZON Research and Innovation Actions Program under Grant Agreement #101080085

3.2 2D Problems

This Section is concerned with 2D benchmark examples. These range from simple extensions of 1D textbook cases to more approaches for segments of battery cooling devices, i.e., the heat exchange in double-bent channel flow, which also includes a grid sensitivity study for laminar and turbulent configurations.

Table 3 summarizes the features of the 2D test cases including a brief outline of the respective focus and the engineering relevance. The focal points refer to (1) the predictive differences between 1D and 2D, (2) more complex vortical flows, (3) applications in curvilinear coordinates and (4) conjugate heat transfer between fluid and solid materials. The governing equation refers to diffusion (D) diffusion reaction (DR), unsteady diffusion (uD), unsteady advection diffusion (uAD), steady advection diffusion (AD), unsteady convection diffusion (uCD) or conjugate heat transfer (CH) problems. One demonstration case employs an algebraic turbulence model (TM). In addition to the classical methods (FD/FV), the Table also contains tensor network methods (TN) as a substep towards QC and possibly additional results obtained from QC methods (Q).

2D Cases	Eqn.	Spatial	Temporal	# Eqn.	non/linear	Flow	# Grids	Num.	Focus	Ind. Relev.
Heat Conduction	(u)DR	2D	un/steady	2	linear	laminar	2	FD+Q	(1)	15%
Lid-Driven Cavities	uAD	2D	unsteady	2	nonlinear	laminar	1	TN	(2)	35%
Curvilinear Cases	uCD	2D	unsteady	1,3	non/linear	lam./TM	1	FD+TN	(3)	35%
S-Bent Ducts	CD/CH	2D	steady	4/6	nonlinear	lam./TM	4	FV	(3,4)	70%
							-			
							-			

TABLE 3: SUMMARY OF SELECTED 2D CASES (3.2).

These cases investigated in Secs. 3.2.2 and 3.2.3 are devoted to quantum-inspired approaches, that have clear links to both, the governing equations and the FD approximations used in classical CFD. The methods employ tensor network strategies to translate the discrete FD approximation of the governing equations. Solutions are not necessarily performed on a QC (or its emulation) but can be performed on a classical computer.

3.2.1 2D Poisson Equation (Un/Steady Heat Conduction) (FD/QCFD)

The 2D un/steady heat conduction is described by a Poisson equation with a source term f, viz.

$$\frac{\partial u}{\partial t} \text{ or } 0 = \nabla^2 u + f, \text{ in a 2D domain } \Omega,$$

with $u = u(x, y)$ and $f = f(x, y)$. The domain refers to a unit square $x, y \in [0,1]\ [m] \times [0,1]\ [m]$. Homogeneous Dirichlet conditions $u = 0$ along all boundaries on a cartesian lattice with 16×16 and 32×32 equidistantly spaced grid points, i.e., $\Delta x = \Delta y = 0.0625\ [m]$ and $\Delta x = \Delta y = 0.03125\ [m]$. Two different source term distributions are investigated in steady conditions, one with a checkerboard source (Sec. 3.2.1.1) and one with a centered Dirac source (Sec. 3.2.1.2). Moreover, the checkerboard source case is used to simulate the initial ten time steps of a unit time interval with $\Delta t = 0.1\ [s]$ of the unsteady case on the fine grid (Sec. 3.2.1.3). The FD results are uploaded and listed under DOI 10.25592/uhhfdm.14241. Next to the FD results, quantum results are given.

Discretization: cartesian, equidistant in space; equidistant in time
Numerics: FD (2nd-order central differences for diffusion, 1st-order backward in time)
Features: 2D, reaction-diffusion scalar transport with Dirichlet boundary conditions
Output: $u(x_i, y_k), u(x_i, y_k, t_j)$,

3.2.1.1 Checkerboard Source

We refer to the above-described steady heat conduction on a rectangular domain with Dirichlet boundary conditions and consider a "checkerboarding" spatial distribution of the source term $(f_h)_{i,j} = f(x_i, y_j)$ as benchmark.

Figure 7 compares the results returned by the VQA with FD results using classical central differences on the fine grid. The left graph shows the source term, while the other two graphs display the quantum solution (center graph) and the classical FD solution (right graph).
The dataset can be found under DOI 10.25592/uhhfdm.14241.

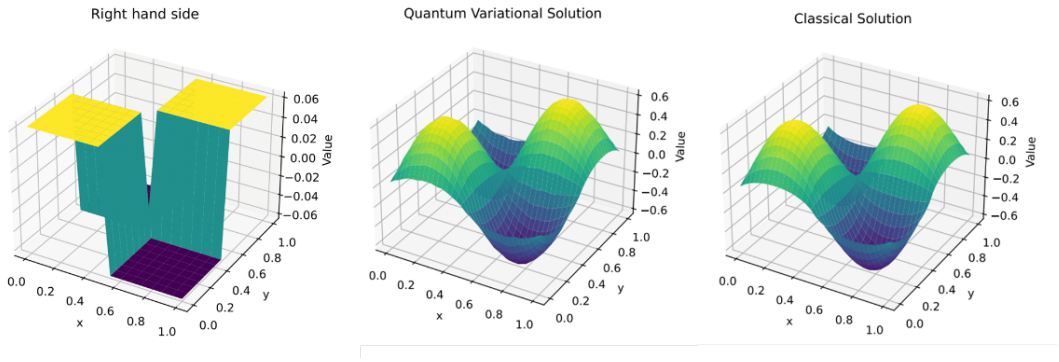

FIGURE 7: RESULTS FOR THE 2D STEADY HEAT CONDUCTION USING A CHECKERBOARD SOURCE (3.2.1.1).

3.2.1.2 Dirac Source

The solution to the steady heat conduction is approximated on the same discretized unit-square domains as in Sec. 3.2.1.1. We again employ the above-mentioned homogeneous Dirichlet boundary conditions. A Dirac impulse $(f_h)_{i,j} = f(x_i, y_j)$, that is centered at Point $P = (0.5\,[m], 0.5[m])$.

The comparison of classical FD (left) and VQA (center) results obtained on the fine grid are provided in Figure 8. The Figure reveals that the quantum results are not symmetric in radial direction. This indicates weaknesses of the ansatz gates used in the variational approach to parameterize the PDE solution. The example serves as an illustration of current QCFD challenges.
The dataset can be found under DOI 10.25592/uhhfdm.14241.

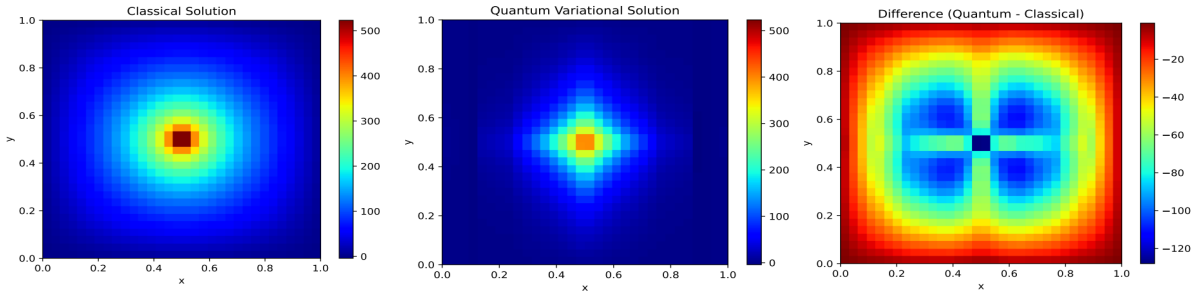

FIGURE 8:RESULTS OF THE 2D STEADY HEAT CONDUCTION USING A DIRAC SOURCE (3.2.1.2).

This project receives funding from the European Union's Horizon 2020 HORIZON Research and Innovation Actions Program under Grant Agreement #101080085

3.2.1.3 Unsteady 2D Heat Transfer (FD/QCFD)

Supplementing temporal changes in combination with cases studied above, the source-free governing equation reads

$$\frac{\partial u(x,y,t)}{\partial t} - \nabla^2 u(x,y,t) - f(x,y,t) = 0,$$

with the initial conditions $u(x,y,0) = u_0$ that follow from the checkerboard solution described in Sec. 3.2.1.1. Again, Dirichlet boundary conditions $u = 0$ are employed (for all times) along the boundaries of a unit square domain discretized on a cartesian grid with 32×32 $(n_x \times n_y)$ equidistantly spaced points ($\Delta x = \Delta y = 0.03125$ $[m]$). Mind that only the first ten time steps were simulated with a fixed step size of $\Delta y = 0.1$ $[s]$.

FD results have been compiled and are supplemented by emulated quantum results and the complete dataset is available via the DOI 10.25592/uhhfdm.14241.

Figure 9 and Figure 10 compare the results for the classical FD solution (right) and a variational quantum solution (left) at time $t = 0.0$ $[s]$ and $t = 0.9$ $[s]$, respectively, on a regular 32×32 $(n_x \times n_y)$ lattice. The x-, y-axes show the number of grid points, whereby the color indicates the corresponding temperature.

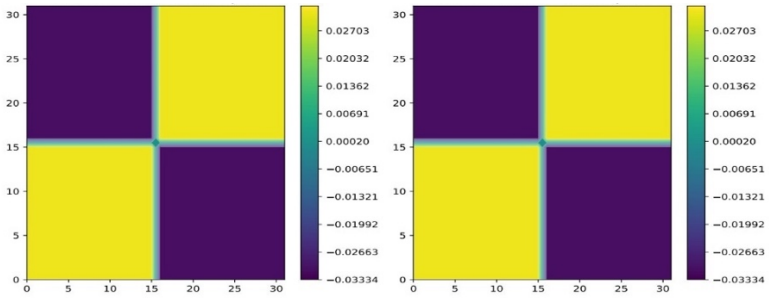

FIGURE 9: RESULTS 2D UNSTEADY HEAT CONDUCTION (3.2.2.) AT $t = 0$ $[s]$ (3.2.1.3).

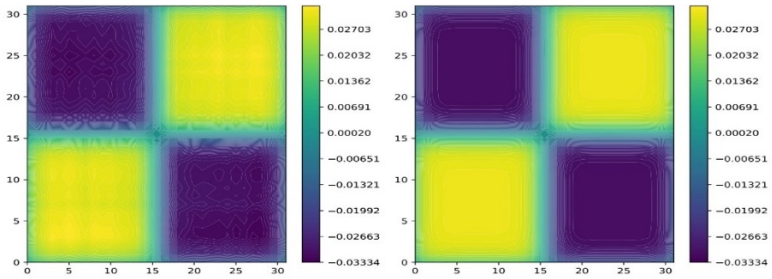

FIGURE 10: RESULTS 2D UNSTEADY HEAT CONDUCTION (3.2.2) AT $t = 0.9$ $[s]$ (3.2.1.3).

3.2.2 Unsteady Lid-driven and Doubly-driven Cavity (QCFD)

The setup for the unsteady lid-driven cavity in two spatial dimensions is shown in Figure 11. We consider a square domain with edge length L, and the upper lid moves with velocity u_0 in the horizontal (x-) direction. The x-component (y-component) of the fluid is denoted by u (v). At $t = 0$ $[s]$, the fluid is at rest, $u = v = 0$ $[m/s]$. We consider a viscous fluid with kinematic viscosity ν and seek steady state solutions to the incompressible Navier-Stokes equations in the stream-function-vorticity approach (cf. [6]).

We scale time in units of $t_0 = L/u_0$, length in terms of L and velocities by u_0. Solutions to the Navier-Stokes equations are then characterized by the Reynolds number $Re = u_0 L/\nu$ which is assigned to 10^3 and 24×10^3. The interior of the cavity (excluding boundaries) is discretized by a uniform cartesian grid with N_p grid points in each

spatial dimension. The computational domain thus comprises $N_p{}^2$ equally spaced points with grid spacing $h = L/(N_p + 1)$. The boundary conditions for u, v, and the stream function ψ and for the lid-driven cavity are shown in Figure 11(b) for the single-driven lid and Figure 11(c) for the doubly-driven lids. In the former case, only the upper lid moves at constant velocity u_0 in the horizontal direction. In the latter case, the bottom lid also moves with an opposite constant velocity -u_0 in the horizontal direction. Solutions are advanced in pseudo time towards steady state using an explicit, second-order accurate McCormack-scheme.

The employed quantum inspired computational methodology has been published by [6]. The dataset for the QCFD results can be accessed via DOI 10.25592/uhhfdm.14235. Mind that the QCFD data has been carefully checked against literature reported classical results, cf. [6].

(a)

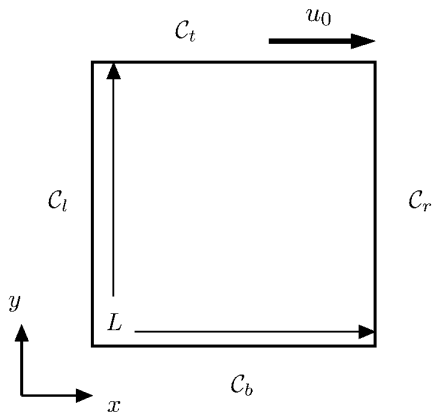

(b)

	$\mathcal{C}_t$	$\mathcal{C}_r$	$\mathcal{C}_b$	$\mathcal{C}_l$
u	u_0	0	0	0
v	0	0	0	0
ψ	0	0	0	0

(c)

	$\mathcal{C}_t$	$\mathcal{C}_r$	$\mathcal{C}_b$	$\mathcal{C}_l$
u	u_0	0	$-u_0$	0
v	0	0	0	0
ψ	0	0	0	0

FIGURE 11: LID-DRIVEN AND DOUBLY-DRIVEN CAVITY-DRIVEN AND DOUBLY-DRIVEN CAVITY (3.2.3).

Discretization: cartesian, equidistant in space; equidistant in time
Numerics: FD (2nd-order central differences for diffusion, 2nd-order central differences for advection)
Features: 2D non-linear convection-diffusion with Dirichlet boundary conditions
Output: $u(x_i, y_j), v(x_i, y_j), \psi(x_i, y_j), \omega(x_i, y_j)$ for the final tine step (at steady state)

3.2.3 Curvilinear Coordinates and LES subsystem demonstrator (FD/QCFD)

The investigations refer to the nonlinear convective transport in a non-rectangular 2D domain using boundary fitted curvilinear coordinates. Moreover, non-constant material properties are considered by the introduction of an algebraic eddy-viscosity model, that relates to the LES Smagorinsky model [8]. The main objective is to reproduce specific classical CFD results, rather than the correct modeling of turbulence physics. Broadening the basis for algorithmic development, the following benchmark case covers two governing equations (Passive Scalar Transport and Navier-Stokes).

As an extension to Sec. 3.1.6 the first case is concerned with a two-dimensional passive scalar transport

$$\frac{\partial \phi}{\partial t} + \vec{u} \cdot \nabla \phi - \Gamma \nabla^2 \phi = 0,$$

for a prescribed velocity $\overrightarrow{u} = 0.5[\cos(\alpha), \sin(\alpha)]^T [m/s]$. The Reynolds number in the (squared) computational domain reads $Re = uL/\Gamma = 500\pi$, based on the length $L = 2\pi$ of the (computational) domain, the maximum

velocity magnitude $u = 0.5\ [m/s]$ and a constant diffusion coefficient $\Gamma = 0.002$. We investigate the evolution of an initial Gaussian pulse $\phi(x, t_0) = A \exp\{[(x - x_0)^2 + (y - y_0)^2]/B\}$ with $A = 1.0$, $B = 0.2$ and $x_0 = \pi, y_0 = \pi$, propagating in a physical domain with periodic boundary conditions along all boundaries.

The problem is solved for four cases, i.e., $\alpha \in$ [0°,45°,90°,140°]. A transfinite interpolation is used to relate a regular squared cartesian lattice $< \xi, \eta >$ to the 2D curvilinear $< x, y >$ physical domain and provide expressions for the cartesian spatial derivatives and metric contributions in a homogeneous computational domain. The computational domain is given by the square $\xi \in [0, L] \times \eta \in [0, L]$, whereby the physical domain is described by $x = \xi - \alpha\, sin(\xi - \eta)$ and $y = \eta - \alpha\, sin(\xi - \eta)$. The computational domain is discretized by 100×100 equidistantly spaced points, i.e., $\Delta\xi = \Delta\eta = 0.01[m]$. The time horizon evolves from $0\ [s]$ to $10\ [s]$. We employ constant time steps of $\Delta t = 0.05\ [s]$ to restrict the Courant numbers to $C_c \leq 1$ and $C_D = 1$.

FD operators are employed to approximate the temporal, convective and diffusive derivatives. Central derivatives are used for all spatial derivatives and 1st-order backward formulae are used in time.

The quantum-inspired strategy (or decomposition) is employed in a tensor network representation based upon a FD method for the differential operators, along with a corresponding relation to capture the metric terms between physical (non-rectangular) and computational (rectangular) domain.

Results of the simulation with the prescribed velocity at $\alpha = 140°$ are given in Figure 12. The FD- and QCFD-data are available via DOI 10.25592/uhhfdm.14169.

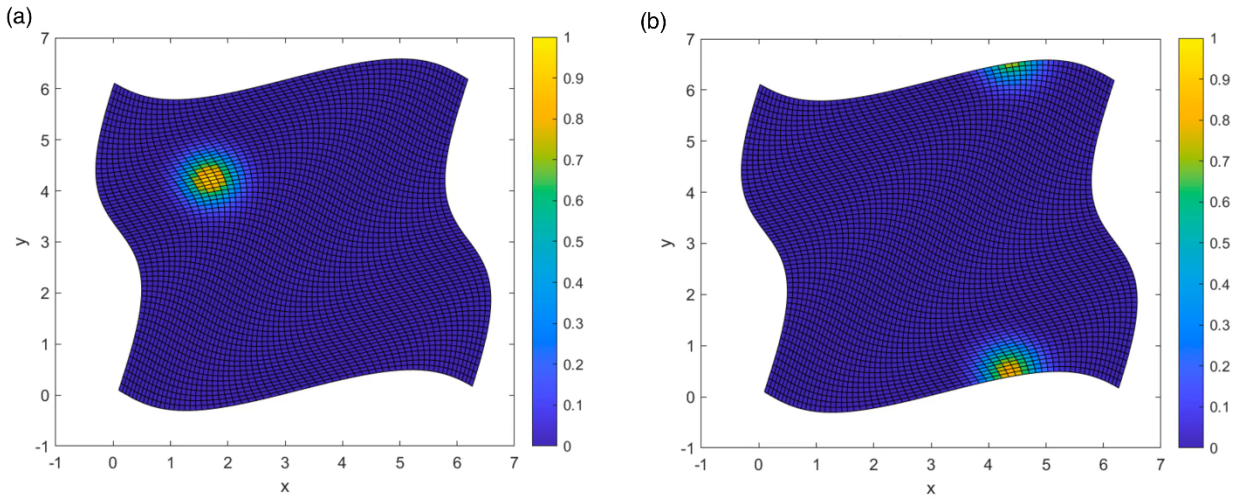

FIGURE 12: SNAPSHOTS OF THE SCALAR FIELD FOR THE GAUSSIAN PULSE EVOLUTION WITH PRESCRIBED VELOCITY AT $\alpha = 140°$ FOR 0.1 [S] (A) AND 0.3 [S] (B) (3.2.3).

In the second study, the application of tensor network methods to curvilinear geometries is extended to Navier Stokes simulations. The simulations employ a fluid viscosity of $\nu = 0.001\ [m^2/s]$ and a spatially variable algebraic eddy viscosity obtained from a Smagorinsky model [8] ($c_s = 0.15$).
The physical domain and its discretization agree with the case described in Figure 12. The time horizon extents from $0\ [s]$ to $10\ [s]$ and the time step reads $\Delta t = 0.05\ [s]$. The simulation employs periodic boundary conditions in the ξ-direction and zero Dirichlet boundary conditions in the η-direction. As initial conditions a parabolic ξvelocity profile is employed along the η-axis across the whole domain. The maximum initial velocity u_{max} at the channel centerline is given by the profile $u(\eta) = -1/\pi^2 \eta\ (\eta - 2\pi)$ and provides $Re = u_{max} L/\nu \approx 6200$.
The pressure is computed using a pressure projection approach to solve a pressure-Poisson equation. The physical domain is the same as in the case described in Figure 12. The solution is advanced in time using an explicit 4th-order

This project receives funding from the European Union's Horizon 2020 HORIZON Research and Innovation Actions Program under Grant Agreement #101080085

Runge-Kutta scheme. The dynamic time step is adaptively chosen to maintain small Courant numbers well below 1. In line with the first application, spatial derivatives are all approximated by central differences.

Figure 13 displays results of the study for the velocity (a), pressure (b) and the divergence of the velocity (c). The FD-data, complementary to the QCFD results, is available at 10.25592/uhhfdm.14169.

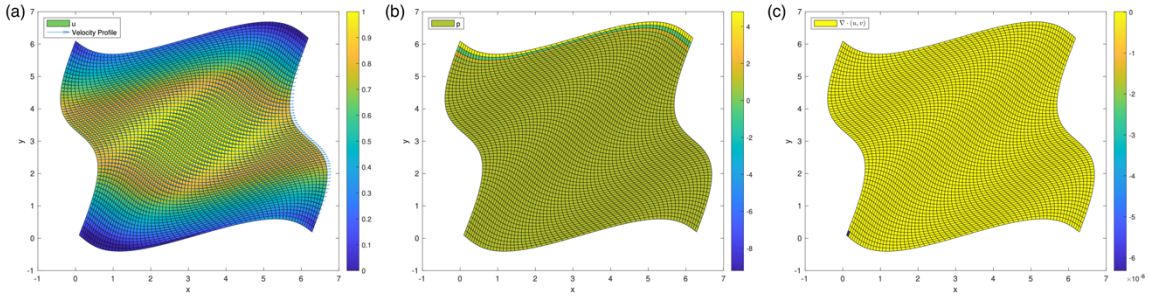

FIGURE 13: VELOCITY (MAGNITUDE), PRESSURE AND DIVERGENCE OF THE VELOCITY WITHIN THE CHANNEL FLOW SIMULATION (3.2.3).

Discretization: curvilinear, equidistant in computational domain
Numerics: FD (2nd-order central differences in space, 4th-order explicit in time)
Features: 2D, nonlinear convection-diffusion transport for momentum and pressure
Output: $u(x_i, y_j, t_k), v(x_i, y_j, t_k), p(x_i, y_i, t_k), x_i, y_j, t_k$

3.2.4 Double-Bent Channel (FV)

The double-bent channel demonstrates a more practical heat transfer problem. Results included in D1.1 cover two generic heat exchanger cases featuring different flow regimes, laminar and (modeled) turbulent flows.

The case consists of a rectangular cross section and is bent follows an "S" shape. The 2D curvilinear domain is one meter long and the height of the bent reads $2\delta = 0.05\ [m]$. The height of the fluid wetted domain refers to delta δ and covers the lower half of the configuration, cf. Figure 14. On top of the fluid partition, an identical partition of solid copper is considered. The inlet velocity of the flow is set to $1\ [m/s]$. The material properties for the fluid (ρ= $1.2\ [kg/m^3]$, $\mu_1 = 5.92 \times 10^{-4} [kg/ms]$, $c_p = 1000\ [J/kgK]$) and solid ($\rho = 8880\ [kg/m^3]$, $\lambda = 401\ [W/m\ \ K]$, $c_p = 386\ [J/kgK]$) are constant over time.

The three dimensionless similarity parameters describing the physics are: (1) the Reynolds number build with the channel half-height $Re = u\delta/\nu = 50$ (laminar) and $Re = 7375$ (turbulent), (2) the Nusselt number $Nu = hL/k \approx 3.45$ (constant for all case) and (3) the Prandtl number $\mathrm{Pr} = \nu\rho c_p/\lambda = 0.7$ (constant for all cases), which describes the relation between the kinematic viscosity and the thermal diffusivity. The latter essentially addresses the ratio between the momentum and thermal boundary layer thicknesses.

The configuration is illustrated in Figure 14. The exterior channel walls are mostly assigned to zero temperature gradient conditions for the energy equation. Exceptions refer to the coolant/fluid inlet ($300\ K$ Dirichlet condition) and the heated lower part of the upper horizontal copper boundary ($500\ K$ Dirichlet condition).
No-slip conditions (zero Dirichlet cond.) are used for the velocities along lower s-Bent exterior walls and the internal cooper/fluid interface. The flow enters the channel with a constant horizontal velocity of $1\ [m/s]$ (and a related ambient temperature of $300\ K$). The fluid outlet refers to a zero-gradient condition for the velocities (and the temperature).

This project receives funding from the European Union's Horizon 2020 HORIZON Research and Innovation Actions Program under Grant Agreement #101080085

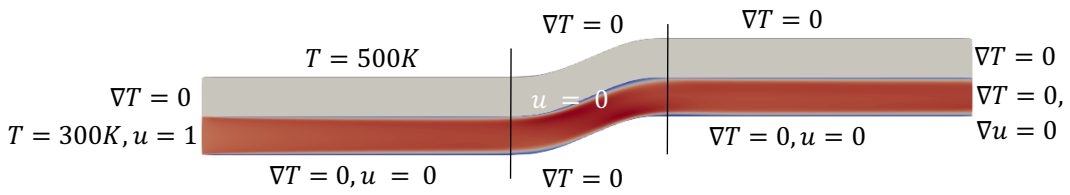

FIGURE 14: SCHEMATIC OF THE TWO-PHASE HEAT TRANSFER IN AN S-BENT PIPE AND BOUNDARY CONDITIONS (3.2.4).

A k-ε RANS turbulence closure model together with a universal wall function approach is used to mimic the influence of turbulence for high Reynolds number case [9].

Both flows are resolved on structured grids, which discretize the fluid and solid domains. To assess the grid resolution a discretization study has been performed using a coarse (6 260 cells), a mid (35 040 cells), a fine (100 160 cells) and an extra fine (400 640 cells) discretization. For all the cases, and in contrast to the regular grid for the solid domain, the fluid grid is refined from the centerline towards the walls by the factor $\beta = 0.2$, viz $\Delta y_{i+1} = \beta \Delta y_i$.
The coarse grid discretizes the solid domain using 1260 cells with the spacing of $\Delta x = 0.016\ [m] \times \Delta y = 0.0025\ [m]$ resulting in 63 streamwise cells and 20 cells in channel height. The fluids domain is approximated using 5000 cells related to a base size for the largest cells of $\Delta x = 0.008\ [m] \times \Delta y = 0.001875\ [m]$. The total number of 5000 fluids cells, separates into 125 cells in streamwise direction and in 40 cells for the opposite section. The finer grid (mid) employs a base size for the largest cells of $\Delta x = 0.00267\ [m] \times \Delta y = 0.0009375\ [m]$ for the fluid domain and a fixed size of $\Delta x = 0.008\ [m] \times \Delta y = 0.00125\ [m]$ for the solid domain. It features 126 (solid) & 350 (fluid) cells in streamwise direction and 40 (solid) & 80 (fluid) cells along the domain height. Accordingly, the fluid domain is discretized with 28 000 cells and the solid domain with 5 040 cells. The (fine) discretization employs 80 000 fluid cells and 20 160 solid cells. The fluids base size is set to $\Delta x = 0.002\ [m] \times \Delta y = 0.000469\ [m]$ and the solids base size to $\Delta x = 0.004\ [m] \times \Delta y = 0.000625\ [m]$. The finest grid is composed from $\Delta x = 0.001\ [m] \times \Delta y = 0.0002343\ [m]$ for the finest fluid cells (320 000 fluid cells) and $\Delta x = 0.002\ [m] \times \Delta y = 0.0003125\ [m]$ for the solid cells (80 640 solid cells). The four discretizations are displayed in Figure 15.

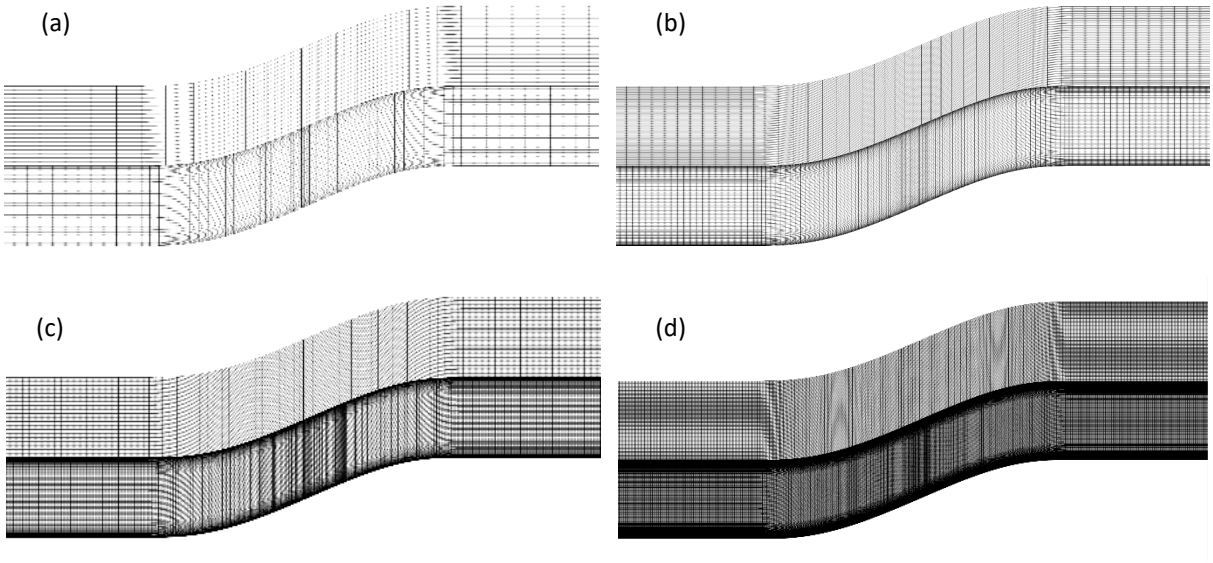

FIGURE 15: DISCRETIZATIONS EMPLOYED IN THE MESH STUDY FOR THE DOUBLE BENT PIPE CASE, FROM LEFT TO RIGHT/TOP TO BOTTOM – COARSE TO EXTRA FINE (A TO D) (3.2.4).

This project receives funding from the European Union's Horizon 2020 HORIZON Research and Innovation Actions Program under Grant Agreement #101080085

For the computation the FV method is established as using cell centered discretization. Integrals of the FV method are approximated using a second-order accurate mid-point rule. Diffusive fluxes are approximated using 2nd-order accurate central differences and convective fluxes employ a centered linear scheme. To assess the convergence of the discretization the total pressure loss along the channels center line is analyzed. The results are given in Table 4 and indicate the mesh independence of the computed flow.

Discretization (Cells)	**Total Pressure Loss Δp $[Pa]$**	
Reynolds Number	$Re = 50$	$Re = 7347$
Coarse (6 260)	4.74705×10^{-3}	3.97777×10^{-4}
Mid (35 040)	4.80524×10^{-3}	4.12331×10^{-4}
Fine (100 160)	4.72851×10^{-3}	4.12331×10^{-4}
Extra Fine (400 640)	4.617750×10^{-3}	4.13059×10^{-4}

TABLE 4: MESH SENSITIVITY STUDY: DOUBLE BENT CHANNEL FLOW.

For each of the combination of Re and discretization the velocity, pressure, temperature fields at steady state and the gird are available via DOI 10.25592/uhhfdm.14199. Different Reynolds numbers or discretizations are indicated in the repository according to the above given order. A more realistic representative fully industrial application, e.g., BEV cooling example, is given in Sec.3.3.2.

Discretization: curvilinear, non-equidistant structured grid in space; steady
Numerics: FV (2nd-order central differences for diffusion, a centered linear scheme for advection)
Features: 2D, turb./lam. nonlinear convection-diffusion with conjugate heat transfer & real. bound. cond.
Output: $u(x_i, y_j), v(x_i, y_j), p(x_i, y_j), T(x_i, y_j), k(x_i, y_j), \epsilon(x_i, y_j), x_i, y_j$ for the solid and the fluid domains

This project receives funding from the European Union's Horizon 2020 HORIZON Research and Innovation Actions Program under Grant Agreement #101080085

3.3 3D Applications

The last set of applications, that the QCFD consortium has selected for future comparisons with QCFD methods, contemplates 3D CFD solutions, i.e., a Taylor-Green vortex (TGV), a 3D periodic channel flow (PCF) and a battery pack cooling scenario.
The description for the TGV case is given in Ref. [5]. It generally follows the classical TGV test case and the data obtained by a quantum-inspired framework is available via DOI 10.25592/uhhfdm.14233.

The remainder of this document describes the channel flow and battery cooling cases. The complexity of both benchmarks is deliberately not set too high in order to correspond to the current state of QCFD and the corresponding hardware capabilities. Table 5 summarizes the 3D test cases and gives information on the main features and the simulation focus. The simulation focus refers to (1) turbulent flow simulation, (2) turbulence modeling - either based on scale-resolving Large Eddy Simulations (LES) or two-equation models for Reynolds-averaged Navier-Stokes (RANS) equations, (3) non-isotropic and non-homogeneous (curvilinear) meshes, and (4) complex internal flows with industrial relevance. The physical phenomena are described by steady or unsteady convection-diffusion (CD/uCD) governed by the Navier-Stokes equations (NS).

3D Cases	Eqn.	Spatial	Temporal	# Eqn.	non/linear	Flow	# Grids	Num.	Focus	Ind. Relev.
Taylor-Green [5]	uCD	3D	unsteady	4	nonlinear	Turb./DNS	2	FD+Q	(1)	25%
Periodic Channel	uCD	3D	unsteady	4	nonlinear	Turb./LES	3	FV	(1,2,3)	50%
Gen. Battery Pack	CD	3D	steady	6	nonlinear	Turb./TM	3	FV	(1,3,4)	90%

TABLE 5: SUMMARY OF SELECTED 3D CASES (3.3).

3.3.1 Periodic Channel Flow (FV)

The period channel flow is an often-performed benchmark to study the interaction of walls and turbulence. Existing studies cover a broad range of Reynolds numbers, including the lower Reynolds numbers studied in the landmark papers [10, 11].
In line with these studies, the geometry is chosen to be a rectangular channel $4\pi\delta \times 2\delta \times 2\pi\delta$, where δ refers to the channel half-height, cf. Figure 16. In the investigated geometry δ is equal to unity, i.e., $1\ [m]$. The discretization's topology is similar to Ref. [10], and subject to a grid sensitivity study outlined below. Simulations are conducted for four laminar and two turbulent flow regimes, specified by the bulk Reynolds numbers $Re_b = \delta u_b/\nu = [150, 300, 600, 1200, 3300, 7890]$, u_b where denotes the spatially averaged velocity aka. bulk velocity. The fluids properties are set to $\nu = 2 \times 10^{-5}\ [s/m^2]$, $\rho = 1\ [kg/m^3]$.
Periodic boundary conditions are employed in the streamwise (x) primary direction and the spanwise (z) lateral direction. Wall boundaries in y-direction correspond to stationary no-slip walls.

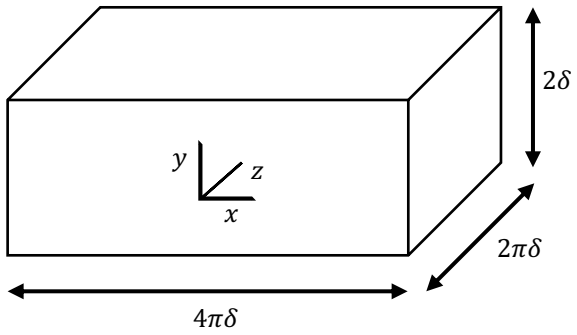

FIGURE 16: SCHEMATIC OF THE PERIODIC CHANNEL FLOW

For the larger Reynolds numbers $Re_b \geq 3300$, a turbulence model is added to the systems of equations providing and approximation to the unresolved sub-grid scales. Here, we employ the LES model by Smagorinsky [8] with the coefficients $c_e = 1.048$ and $c_k = 0.094$. Mind that, no specific wall model is introduced to adjust to the near wall regime, and the flow is described with the algebraic Smagorinsky eddy-viscosity model in the entire domain. This is certainly debatable from a physical point of view. However, the project does not aim to supplement the rich body of outstanding existing channel simulation data available in literature, rather to provide a database for the comparison of QCFD and CFD.
The flow is therefore driven by a prescribed momentum source in the streamwise (x) direction which follows from constant mass flux ($\rho u_b A = \int_{\text{inlet}} \rho u \, dA$). Initial conditions are set to constant inflow axial velocities u_b. A large simulation time $T = 150 \cdot (4\pi\delta)/u_b$[s] is computed to guarantee the full transition of the flow from the initial transient phase into the periodic phase.

Results were obtained from a cell-centered FV scheme. Integrals are approximated using a 2nd-order accurate mid-point rule. The time derivatives are discretized using an implicit 1st-order Euler scheme. Diffusive fluxes follow from 2nd-order accurate central differences and a centered linear scheme for the approximation of convection fluxes. Pressure information is recovered using a semi-implicit method for pressure linked equations (SIMPLE). The three discretization levels account for 30 720 cells 60 000 cells, and 100 800 cells. All the grids are depicted in Figure 17. For all the case the discretizations are refined from the centerline to the wall by the factor $\beta = 0.125$, viz $\Delta y_i = \beta \Delta y_{i+1}$. The grid characteristics is assessed with the non-dimensional inner coordinate of the first interior cell centroid, i.e., $y_1^+ = \rho u_\tau y_1/\nu$ using an empirical wall shear-stress velocity $u_\tau = \sqrt{\frac{\tau_w}{\rho}}$. Therein, an empirical value for the wall-shear stress τ_w was used for laminar flows [11, 12, 13], viz. $\tau_w = 6\rho u_b^2/Re_b$. For the turbulent regime, Deans' correlation was applied to specify the wall shear $\tau_w = 0.073 Re_b^{-1/4} \frac{1}{2} \rho u_b^2$ [12]. This yields y_1^+ values between $y_1^+ \in [1.1, 2.1]$ for the lowest Re number and $y_1^+ \in [2.4, 4.5]$ for the largest Re number for the three grids.

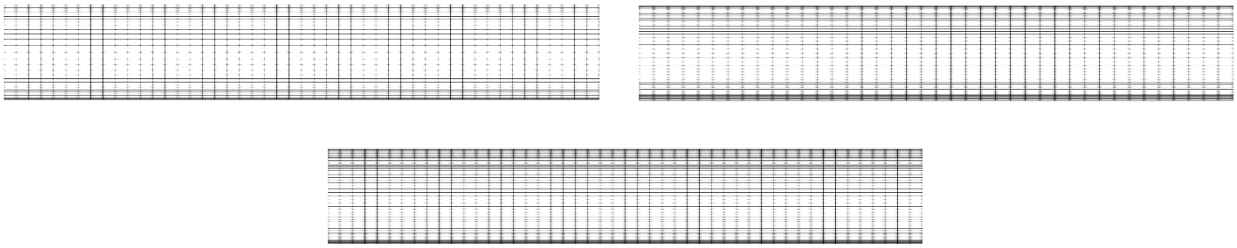

FIGURE 17: DISCRETIZATIONS EMPLOYED IN THE MESH STUDY FOR THE PERIODIC CHANNEL FLOW, FROM LEFT TO RIGHT/TOP TO BOTTOM – COARSE TO FINE (3.3.1).

The coarsest discretization (coarse) is recovered using a base x-spacing of $0.2617\ [m]$, a y-spacing of $0.1452\ [m]$ and a z-spacing of $0.314\ [m]$. It employs $48 \times 32 \times 20$ cells, respectively. With the refinement towards the nonslip boundaries the discretization covers the near wall behavior up to a $y_1^+ = 2.08$ ($Re = 150$) or $y_1^+ = 4.46$ ($Re = 7890$) (y-direction). The medium discretization (mid) has a base mesh of $\Delta x \times \Delta y \times \Delta z = 0.31415\ [m] \times 0.09364\ [m] \times 0.2094\ [m]$ and consists of $40 \times 50 \times 30$ cells resulting in $y_1^+ = 1.34$ for $Re = 150$ and $y_1^+ = 2.88$ for $Re = 7890$. The finest discretization (fine) employs $48 \times 60 \times 35$ cells with a base mesh size of $\Delta x = 0.2618\ [m]$, $\Delta y = 0.0783[m]$ and $\Delta z = 0.17940\ [m]$. With the refinement towards the walls, the y_1^+ values in wall normal direction are between $y_1^+ = 1.12$ and $y_1^+ = 2.4$, for the above given minimum and maximum Reynolds numbers, respectively. In z-direction all of the cases fulfill a $z_1^+ \leq 50$.

The boundary layer displacement thickness is defined as the integral of the normalized velocity deviation over the half channel height, viz. $\delta^* = \sum_{y=0}^{\delta} (1 - u/u_b)$ .To analyze the quality of the discretizations, the boundary layer displacement thickness at the middle of the channel's centerline is evaluated. Therefore, the time averaged x-

component of the velocity along the line $(0, s, 0) : s \in [0, \delta]$ is used. The quantitative results for 18 cases, covering all Reynolds numbers for the three discretizations (coarse, mid, fine), are listed in Table 6.

Reynolds Number	**Displacement Thickness $\delta^*[m]$**		
Discretizations/Cells	Coarse /30,720	Mid / 60,080	Fine / 100,000
$\boldsymbol{Re = 150}$	0.3333	0.3337	0.3338
$\boldsymbol{Re = 300}$	0.3333	0.3337	0.3338
$\boldsymbol{Re = 600}$	0.3309	0.3323	0.3338
$\boldsymbol{Re = 1200}$	0.3142	0.3210	0.3175
$\boldsymbol{Re = 3300}$	0.3259	0.3172	0.2982
$\boldsymbol{Re = 7890}$	0.3083	0.2937	0.2387

TABLE 6: GRID SENSITIVITY STUDY: PERIODIC CHANNEL FLOW (3.3.1).

Mind that when Dean's correlation of centerline and bulk velocities is analyzed (viz. $u_c/u_b \approx 1.16$ $(Re = 7890)$) [10], the simulation results deviate from the correlation data. This is due to the fact that no specific wall treatment is used, but should not detract from the verification study, cf. statement above.

Following a successful verification, the QCFD model can be extended to higher complexity by advanced LES approaches (Van Driest, Cube-root Volume, Wall Adapting Local Eddy-viscosity (WALE), or other) or by employing a wall-function approach to cover the near wall behavior more accurately. For validation, the results for all combinations of Reynolds numbers and discretization are given. Access to the data is granted via DOI 10.25592/uhhfdm.14195.

Discretization: non-equidistant structured grid in space; unsteady
Numerics: FV (2nd-order central differences for diffusion, centered linear scheme for convection)
Features: 3D, turbulent, non-linear convection-diffusion with resolved turbulence content
Output: $u(x_i, y_j, t_k), v(x_i, y_j, t_k), p(x_i, y_j, t_k), \nu_t(x_i, y_j, t_k), x_i, y_i, t_k$

3.3.2 Battery Pack Cooling (FV)

The last case of D1.1 prepares to address a problem relevant to battery electric vehicles (BEVs) and the automotive industry, namely the thermal management of a battery pack. To this end, the following scenario recovers the fluid dynamic (momentum) problem within the cooling device of a battery pack thermal management system depicted in Figure 18 .

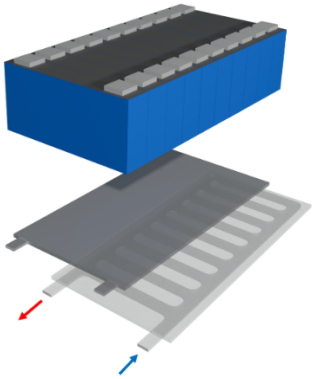

FIGURE 18: SIMPLIFIED THERMAL MANAGEMENT SYSTEM FOR A BATTERY PACK (3.3.2).

The thermal management system of a battery pack is modelled with three regions: (1) coolant channel of 3 $[mm]$ height filled with water, (2) aluminum plate of 4 $[mm]$ thickness and (3) ten battery cells. This deliverable is confined to the pure momentum problem within the coolant channel of $a = 3\ [mm]$ height and $b = 12\ [mm]$ width. The coolant takes the material properties of water ($\rho = 996.57\ [kg/m^3]$, $\mu = 8.53 \times 10^{-4}\ [m^2/s]$). The flow enters the inlet, indicated by the blue arrow, and leaves the domain at the outlet (red arrow), cf. Figure 18.

The data covers a laminar and turbulent flow case. The Reynolds number, defined with the hydraulic diameter of the rectangular cross section $D_h = 2ab/(a+b)$ and the bulk velocity u_b, reads $Re = \rho u_b D_h/\mu = 560$ for the laminar case and $Re = \rho u_b D_h/\mu = 11\,240$ for the turbulent flow case, respectively.
Computed results were obtained from a cell centered FV scheme. Integrals are approximated using a second-order accurate mid-point rule. The time derivatives are discretized using an implicit 1st-order Euler scheme. Diffusive fluxes follow from 2nd-order accurate central differences and a centered linear scheme for the approximation of convection fluxes. Pressure is obtained from a semi-implicit method for pressure linked equations (SIMPLE). The turbulent flow simulations utilize a linear two-equation eddy-viscosity (RANS) model, i.e., the $k-\omega$ SST model [14].
To assess the grid quality, again three different structured-grid discretizations have been assessed. The basis of the fine grid consists $400 \times 200 \times 10$ cells and a cell size of $\Delta x = 0.75\ [mm] \times \Delta y = 0.75\ [mm] \times \Delta z = 0.75\ [mm]$. This basis is successively coarsened in each direction by factor $\sqrt{(2)}$ to obtain a mid-size and a coarse grid basis. Moreover, three near-wall layers are added to each mesh, where the fluid adjacent employs a height of 30% of the base size and refines with factor 0.75 towards the wall. The sensitivity study thereby employs a coarse grid (197,478 cells), a mid-size grid (386,328 cells) and a fine grid (914,040 cells). A closeup view on important regions of the discretization is given in Figure 19.

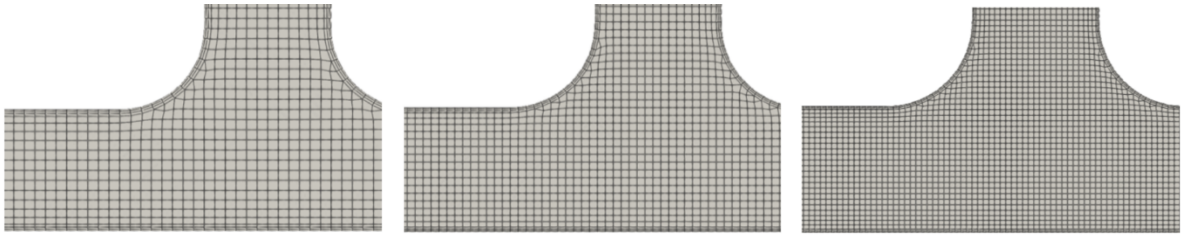

FIGURE 19: DISCRETIZATIONS EMPLOYED IN THE MESH STUDY FOR THE BATTERY COOLING CASE, LEFT TO RIGHT - COARSE TO FINE (3.3.2).

To quantify the grid sensitivity the total pressure loss between inlet and outlet was computed, cf. Table 7. Minor variations of the total pressure loss confirm the reliability by the given discretizations. The data is available online via DOI 10.25592/uhhfdm.16639.

Within D2.1. it is planned to extend this application by conjugate heat transfer simulations, cf. Sec 3.2.4, to assess a complete 3D battery cooling scenario.

Discretization / Cells	**Total Pressure Loss Δp $[Pa]$**	
Reynolds Number	$Re = 560\ (\mu_1)$	$Re = 11240\ (\mu_2)$
Coarse/ 197,478	28.69	3049.6
Mid/ 386,328	28.15	3094.8
Fine / 914,040	28.33	3077.7

TABLE 7: MESH SENSITIVITY STUDY: COOLANT PLATE IN A BATTERY PACK

Discretization: non-equidistant structured grid in space with refinement layers; steady
Numerics: FV (2nd-order central differences for diffusion, a linear central scheme for convection)
Features: 3D, turbulent, nonlinear convection-diffusion with realistic geometry, and boundary conditions
Output: $u(x_i, y_j), v(x_i, y_j), p(x_i, y_j), k(x_i, y_j), \omega(x_i, y_j), x_i, y_j$

This project receives funding from the European Union's Horizon 2020 HORIZON Research and Innovation Actions Program under Grant Agreement #101080085

References

[1] D. Jaksch, P. Givi, A. J. Daley and T. Rung, “Variational Quantum Algorithms for Computational Fluid Dynamics,” *AIAA Journal,* vol. 61, pp. 1885-1894, 2023.

[2] P. Over, S. Bengoechea, T. Rung, F. Clerici, L. Scandurra, E. de Villiers and D. Jaksch, “Boundary Treatment for Variational Quantum Simulations of Partial Differential Equations on Quantum Computers,” *Computers & Fluids,* vol. 288, 2024.

[3] P. Over, S. Bengoechea, P. Brearley, S. Laizet and T. Rung, *Quantum Algorithm for the Advection-Diffusion Equation with Optimal Success Probability,* Preprint arXiv, 2024.

[4] S. Bengoechea, P. Over, D. Jaksch and T. Rung, *Towards Variational Quantum Algorithms for generalized linear and nonlinear transport phenomena,* Preprint arXiv, 2024.

[5] N. Gourianov, M. Lubasch, S. Dolgov, Q. Y. van den Berg, H. Babaee, P. Givi, M. Kiffner and D. Jaksch, "A quantum-inspired approach to exploit turbulence structures," *Nature Computational Science,* vol. 2, p. 30–37, 2022.

[6] M. Kiffner and D. Jaksch, “Tensor network reduced order models for wall-bounded flows,” *Physical Review Fluids,* vol. 8, p. 124101, 2023.

[7] J. H. Ferziger, M. Perić and R. L. Street, Computational Methods for Fluid Dynamics, Springer, 2019.

[8] J. Smagorinsky, “General Circulation Experiments with the Primitive Equations - I. the Basic Experiment,” *Monthly Weather Review,* vol. 91, pp. 99-164, 1963.

[9] B. Launder and D. Spalding, “The numerical computation of turbulent flows.,” *Computer methods in applied mechanics and engineering,* vol. 3, p. 269–289, 1974.

[10] J. Kim, P. Moin and R. Moser, “Turbulence statistics in fully developed channel flow at low Reynolds number,” *Journal of Fluid Mechanics,* vol. 177, p. 133–166, 1987.

[11] R. D. Moser, J. Kim and N. N. Mansour, “Direct numerical simulation of turbulent channel flow up to Reτ=590,” *Physics of Fluids,* vol. 11, pp. 943-945, 1999.

[12] R. B. Dean, “Reynolds Number Dependence of Skin Friction and Other Bulk Flow Variables in Two-Dimensional Rectangular Duct Flow,” *Journal of Fluids Engineering,* vol. 100, no. 02, pp. 215-223, 1978.

[13] H. Schlichting and K. Gersten, Boundary-Layer Theory, Springer, 2016.

[14] F. Menter, M. Kuntz and R. Langtry, “Ten years of industrial experience with the SST turbulence model,” in *In Proceeedings of the fourth international symposium on turbulene, heat and mass transfer*, 2003.

This project receives funding from the European Union's Horizon 2020 HORIZON Research and Innovation Actions Program under Grant Agreement #101080085